Langmuir

Article

pubs.acs.org/Langmuir

# Interstratification Patterns from the pH-Dependent Intercalation of a Tetracycline Antibiotic within Montmorillonite Layers

Ludmilla Aristilde,*[,†] Bruno Lanson,[‡] and Laurent Charlet[‡,§]

[†]Biological and Environmental Engineering, Cornell University, Ithaca, New York 14850, United States

[‡]Institut des Sciences de la Terre, ISTerre, University of Grenoble-1, CNRS, F-38041 Grenoble, France

[§]Institut Universitaire de France, 75005 Paris, France

Supporting Information

**ABSTRACT:** Little is known about the distribution of the intercalated molecules within the interstratified layers resulting from the pH-dependent interlayer adsorption of ionizable organic molecules, including antibiotics, within smectite-type clay minerals. Here we employed experimental and simulated X-ray diffraction (XRD) to characterize interstratification (or mixed layering) from the intercalation of oxytetracycline (OTC), a commonly used tetracycline antibiotic, within Na-montmorillonite layers at pHs 4, 5, 6, and 8. Our XRD data reveal that OTC is distributed nonrandomly in the interlayers such that Na- and OTC-saturated interlayers coexist. The profile of the full width at half-maximum intensity (fwhm), monitored as a function of increasing layer-to-layer distance ($d_{001}$), resulting from an increasing amount of intercalated OTC, reflects such mixed-layer crystals under the acidic pH conditions. A minimum in fwhm occurs at a d spacing of about 1.8 nm, which is to be the optimal $d_{001}$ for OTC-saturated layers, in agreement with molecular modeling results. Using the coordinates of the thermodynamically favorable configuration of the adsorptives in a model montmorillonite interlayer, we simulated XRD profiles to unravel the different patterns of interstratification from the experimental data. At both pHs 4 and 5, Na- and OTC-interlayers are randomly interstratified, whereas at pH 6, these layers are clustered, as characterized by a segregated interstratification pattern. The theoretical layer stacking sequences of the simulated XRD illustrate, as pH increases, the clustering of similar layer types with the exclusion of OTC intercalation from clay populations enriched in Na. At pH 8, both fwhm and $d_{001}$ indicate OTC adsorption primarily on external surface sites, not within interlayers. Our findings imply that, in addition to chemical speciation, a pH-dependent formation of montmorillonite crystallites with unexfoliated layers may be responsible both for the decreased OTC intercalation and for the increased binding on external sites, thus resulting in the different patterns of interstratification as a function of increasing pH.

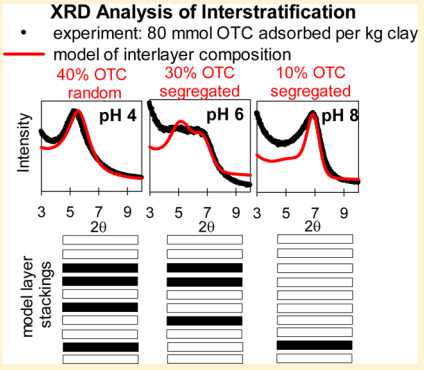


## INTRODUCTION

In natural soils and engineered materials, clay minerals can play an important role in the retention of metal cations and polar organic molecules that can participate in cation-exchange and surface complexation reactions. The intercalation behavior of these adsorptives within layers of smectite-type clay minerals is of special interest due to the importance of these clays both in environmental fate and as candidates for remediation strategies. The lack of homogeneous distribution of intercalated species and the corresponding observation of different interstratification patterns have been well-documented for the adsorption of a mixture of metal cations on smectites.[1−5] From the different hydration states of the cations under specific relative humidity conditions,[5−7] it was deduced that a smectite typically hosts different cations in different interlayers, a process termed "demixing" in the early works by Méring and Glaeser.[1] Demixing refers to when the population of exchangeable cations in an interlayer is different from the average population of these cations in the whole sample. For instance, the XRD data for mixed Ca−Na smectite clays[1,2,5] imply demixing of the adsorbed ions such that some interlayers contain mostly Na while others contain mostly Ca. Random interstratification of the demixed layers is typical in most cases and is characterized by the evolution of a single 001 peak, accompanied by peak broadening, between the diffraction peaks of the pure Na and Ca clays.[1−5] Segregated and ordered patterns of the different interlayer types in mixed layered smectites have also been reported (see ref 8 and references therein). Segregated interstratification[8] refers to some degree of clustering in the stacking sequences of the de-mixed layers such that, for instance in the case of Ca−Na smectites, two Ca-rich interlayers would be more likely adjacent than expected for a random interstratification; ordered interstratification minimizes the consecutive occurrence of the minor layer type. The XRD patterns of segregated mixed layers are typically characterized by two 001 peaks in the XRD patterns, as a result of the increased abundance of layer pairs and triplets corresponding to discrete domains of each layer type.[8] The aforementioned different interstratification behavior is also implied from

**Received:** September 7, 2012
**Published:** March 25, 2013

diffraction patterns of smectite minerals intercalated with polar organic molecules.[9−18] However, a characterization of these interstratified structures is still largely lacking.

Adsorption studies of various alkylammonium cations on vermiculites[9] and smectites[9−11] and of antibiotics on a smetitic soil,[12] a rectorite,[13] a mica-montmorillonite (mica-MONT),[14] a hectorite,[14] and a MONT[14−18] demonstrated how differences in the identity of the adsorptive molecules, the type of clay adsorbent, and the population of the adsorbate species can lead to different interstratification patterns. The origin of the different stacking sequences in mixed layer smectites remains largely unknown, but it has been proposed that the ordering (or lackthereof) of the interstratified interlayers may be dependent on the aqueous conditions such as ionic strength and pH, the localization of the structural charges on the clay (i.e, type of clay), the identity and population of the adsorbed species, and the hydration states of the layers (7, 8, 19 and references therein). A characterization of the evolution of the interstratified structures as a function of both the amount of adsorbed species and the pH is requisite toward a comprehensive understanding of the factors controlling the physical exclusion of ionizable organic molecules within the interlayers of smectite-type clays in natural and engineered systems.

With a focus on the tetracycline (TET) antibiotics, an important class of protein synthesis inhibitors widely used in both human and veterinary medicine, it is evident from XRD that the intercalation of these antibiotics within smectite layers is dependent on pH, whereby there is an increase in the layer-to-layer distance ($d_{001}$) under acidic pH conditions; however, minimal intercalation is observed under circumneutral and basic pH conditions.[12,15,20−26] Furthermore, this pH-dependent intercalation correlates positively with the extent of adsorption of TETs on MONT.[16] These results thus imply that access to interlayers and interlayer adsorption both are promoted by favorable speciation of the adsorptive molecules, which are increasingly cationic as pH decreases. However, in addition to chemical speciation, recent studies indicate that structural insights may be required in order to fully decipher the mechanisms of TET intercalation within the smectite clay layers. A nuclear magnetic resonance (NMR) examination[16] of the molecular environments of MONT-associated $^{23}$Na in the presence of intercalated TET species reveals the presence of undisturbed interlayer Na cations, indicating a preferential localization of the antibiotic species in specific interlayers. And, XRD studies of the adsorption of TETs[12−14] and other molecules [lincomycin,[17] lysine,[18] ciprofloxacin[27]] by smectite clays report a broadening of the 001 peak as a function of increasing $d_{001}$, which is consistent with the interstratification, or mixed layering, of smectite interlayers with and without the intercalated molecules. Furthermore, a study on the adsorption of TET compounds on Na-MONT reported XRD patterns in which there was a single 001 peak under acidic pH conditions[15] but two peaks under circumneutral to basic pH conditions,[14,15] suggesting different patterns of interstratification as a function of pH. These changes in the peak morphology have not been fully investigated, and their implications in understanding the interstratification pattern of the antibiotic-containing layers have not been resolved.

Here, we build on the previous findings on the pH-dependent intercalation of TETs within MONT and employ both simulated and experimental XRD to characterize the interstratification patterns from the adsorption of oxytetracycline (OTC, Figure 1) on Na-MONT at pHs 4, 5, 6, and 8. Changes in the full width at half-maximum intensity (fwhm) of

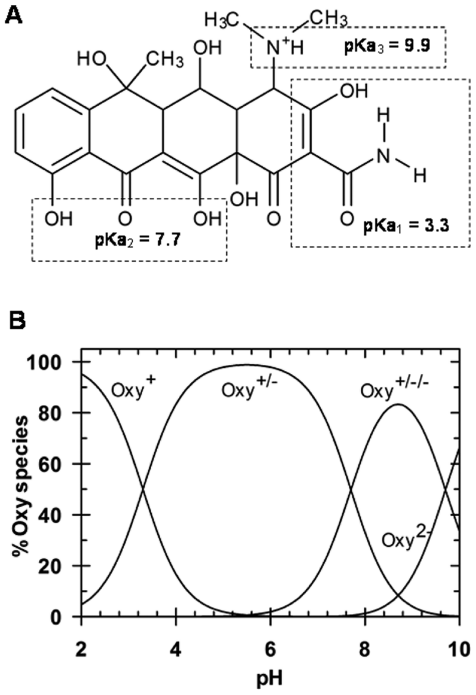


**Figure 1.** (A) Schematic structure and (B) ionization scheme of oxytetracycline (OTC).

the peaks (i.e., peak broadening) as a function of $d_{001}$ values (i.e., as a function of the amount of intercalated OTC) were monitored in order to determine the optimal $d_{001}$ for the molecular simulations of the interlayer adsorption. A Monte Carlo search approach combined with geometry optimization and molecular dynamics algorithms was employed to obtain optimized interlayer conformations for the simulation of XRD profiles, assuming layer stacking sequences corresponding to either random interstratification or segregated interstratification. Guided by the simulated XRD profiles and their corresponding compositional signature, the different patterns of interstratification were characterized as a function of pH. In using coordinates from optimized structures to simulate XRD profiles, our study seems to be the first study, to the best of our knowledge, to combine molecular modeling simulations with X-ray diffraction explicitly to resolve the structures underlying the intercalation behavior of organic molecules within clay layers.

## MATERIALS AND METHODS

**Materials.** Oxytetracycline-hydrochloride (>99%) and all other chemicals (analytical grade) were purchased from Sigma-Aldrich. The Na-MONT [$Na_{0.60}Si_8(Al_{3.40}\ Mg_{0.60})O_{20}(OH)_4$] was synthesized as described previously[28] and has an XRD pattern similar to Wyoming-type Na-MONT.[29]

**Adsorption Experiments.** Adsorption isotherms of OTC on the clay were performed, as previously described,[12] by adding 20.0 mL of OTC solutions (0.01, 0.03, 0.05, 0.1, 0.2, 0.32, 0.5, 0.75, or 1 mM) to 0.02 g of clay in PTFE tubes, which were kept in the dark by being covered with aluminum foil in order to prevent light-mediated side reactions. The OTC solutions were prepared in 0.01 M $NaNO_3$ ionic medium with 5 mM each of an acetate/bicarbonate ($NaCH_3COO$/


dx.doi.org/10.1021/la400598x | Langmuir 2013, 29, 4492−4501

$NaHCO_3$) buffer, brought to pHs 4, 5, 6, or 8. With the use of a UV−vis spectrophotometer (Perkin-Elmer Lamda35), the concentration of OTC in solution was determined, following centrifugation, of the OTC-clay suspension and filtration of the supernatant through a 0.22 $\mu$m polycarbonate filter (Fisher). Blank experiments revealed that less than 5% of the OTC was lost by adsorption to the tube and the filter.

**X-ray Diffraction Measurements.** For XRD analysis of the samples from the adsorption experiments, oriented slides were prepared by pipetting the clay slurry onto a glass slide, following the centrifugation step described above. Independent experiments were performed to ascertain that there were no appreciable changes in the 001 reflection in the presence of only the buffer compounds under the different pH conditions (data not shown). Therefore, observed changes in the XRD patterns were attributed to be a result of antibiotic intercalation. High temperatures may influence the stability of the intercalated antibiotic,[13] and the relative humidity (RH) conditions control smectite hydration states[30] with subsequent implications for the interpretation of the XRD patterns.[12] Thus, to avoid experimental artifacts, oriented samples were equilibrated and measured at constant temperature (25 °C) and RH (20%). The latter value was chosen to optimize the $d_{001}$ contrast between Na- and OTC-exchanged layers. All XRD patterns were recorded with a Bruker D5000 diffractometer operated at 40 kV and 40 mA and equipped with a SolX solid-state detector from Baltic Scientific Instruments and an Ansyco rh-plus 2250 humidity control device coupled to an Anton Paar TTK450 chamber. The scanning parameters were 0.02° 2$\theta$ step size and 8 s as counting time per step over the 2−10° 2$\theta$ Cu K$\alpha$ angular range ($\lambda$ = 1.5418 Å); preliminary XRD measurements revealed a lack of well-defined peaks at higher 2$\theta$ angles.

**Molecular Modeling.** In preparation for the simulation of XRD profiles, we performed molecular simulations of Na- and OTC-saturated MONT layers (henceforth termed Na interlayer and OTC interlayer, respectively) to determine the interlayer organization of the adsorptive species (Na, cationic OTC, water) within a model MONT $[Na_{0.5}(Si_8)(Al_{3.5}Mg_{0.5})O_{20}(OH)_4]$ (Figure 2). The 2.112 × 1.828 × $d_{001}$ nm$^3$ cell contains a total charge of −4, resulting from four isomorphic substitutions in the octahedral sites (Al → Mg) in accordance with the MONT used in the adsorption experiments. The specific $d_{001}$ values of 1.2575 nm for the Na interlayer and 1.8 nm for the OTC interlayer were deduced from XRD data (see Results and Discussion). We note here that our XRD data indicate about 1.8 nm optimal layer spacing for the OTC interlayer at pHs 4, 5, and 6, thus suggesting a similar interlayer environment for the intercalated environment at the different pH values (see Results and Discussion). Furthermore, previous examinations of OTC−MONT complexes using both infrared (IR) and NMR spectroscopies imply similar binding conformation of OTC on the clay surface at different pH values (see Results and Discussion). Thus, the optimized configuration of the bound cationic OTC in the model MONT interlayer at a $d_{001}$ of 1.8 nm (Figure 2B) was considered adequate to generate the simulated XRD profiles. We also posit that any minimal changes that would arise from the electronic density distribution of the precise configuration of adsorptive molecules would likely be diffused over the whole interlayer region and not influence the calculated XRD patterns.

The Na interlayer consists of 4 Na and 38 $H_2O$ molecules, and the OTC interlayer had 2 cationic OTC molecules, 2 Na ions, and 56 water molecules. The water content for the interlayers at 20% RH was estimated from previously determined hydration properties of a MONT as a function of RH.[30] Due to steric constraints, only a maximum of two OTC molecules (i.e., 348 mmol OTC kg$^{-1}$ clay) were allowed in the interlayer space of the simulated cell; this value is lower than the measured permanent structural charge [440 mmol$_c$ kg$^{-1}$].[31] The partial charges of the water atoms were according to the extended simple point charge water model;[32] those of the MONT atoms were taken from the CLAYFF model,[33] and all other atom descriptions and bonding and nonbonding terms were according to the condensed-phase optimized molecular potentials for atomistic simulation studies (COMPASS) force

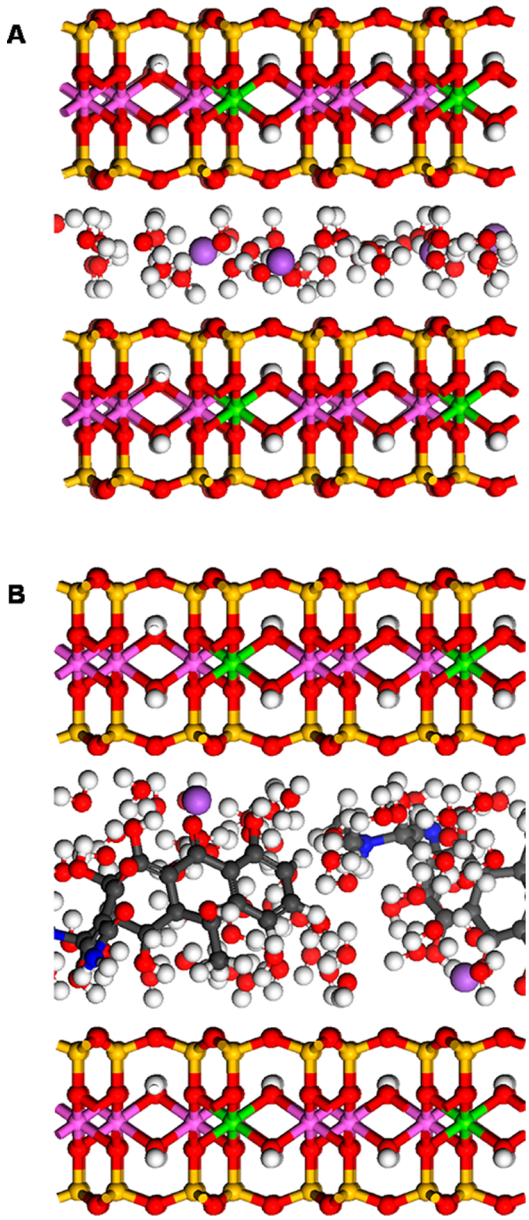


**Figure 2.** Views of the optimized adsorptive structures of (A) 4 Na and 2 OTC and (B) 2 Na located within a hydrated interlayer of a model MONT at $d_{001} \approx 1.26$ nm and $d_{001} = 1.80$ nm, respectively. In each panel, the clay structure at the bottom is a periodic image of the one at the top. The OTC and water molecules and the clay structure are shown in a ball-and-stick motif, and the Na ions are represented by small spheres. Color code: gray (C), red (O), white (H), blue (N), yellow (Si), pink (Al), green (Mg), and purple (Na).


dx.doi.org/10.1021/la400598x | Langmuir 2013, 29, 4492−4501

Table 1. Results of Adsorption Experiments and X-ray Diffraction Measurements at pHs 4, 5, 6, and 8[a]

| pH 4 | | | | pH 5 | | | | pH 6 | | | | pH 8 | | | |
|---|---|---|---|---|---|---|---|---|---|---|---|---|---|---|---|
| Q | $d_{001}$ | $\Delta d$ | fwhm | Q | $d_{001}$ | $\Delta d$ | fwhm | Q | $d_{001}$ | $\Delta d$ | fwhm | Q | $d_{001}$ | $\Delta d$ | fwhm |
| 0.0 | 1.25 | – | 1.21 | 0.0 | 1.26 | – | 1.23 | 0.0 | 1.25 | – | 1.32 | 0.0 | 1.27 | – | 1.32 |
| 9.8 | 1.29 | 0.04 | 1.42 | 9.5 | 1.29 | 0.03 | 1.45 | 6.6 | 1.26 | 0.01 | 1.40 | 15.3 | 1.26 | 0.01 | 1.22 |
| 10.5 | 1.30 | 0.05 | 1.36 | 9.6 | 1.28 | 0.02 | 1.34 | 7.4 | 1.26 | 0.01 | 1.30 | 32.9 | 1.26 | 0.01 | 1.34 |
| 26.7 | 1.27 | 0.02 | 1.30 | 48.4 | 1.49 | 0.23 | 1.90 | 7.4 | 1.27 | 0.02 | 1.46 | 54.7 | 1.27 | 0.00 | 1.22 |
| 40.7 | 1.56 | 0.31 | 1.51 | 48.8 | 1.46 | 0.20 | 1.96 | 28.5 | 1.30 | 0.05 | 1.89 | 67.5 | 1.27 | 0.00 | 1.22 |
| 49.6 | 1.51 | 0.26 | 1.55 | 73.4 | 1.59 | 0.33 | 1.69 | 30.4 | 1.28 | 0.03 | 1.52 | 77.7 | 1.28 | 0.01 | 1.36 |
| 52.1 | 1.52 | 0.27 | 1.57 | 87.4 | 1.61 | 0.35 | 1.33 | 33.4 | 1.29 | 0.04 | 1.70 | 80.8 | 1.28 | 0.01 | 1.27 |
| 78.4 | 1.61 | 0.36 | 1.36 | 127.3 | 1.72 | 0.46 | 1.13 | 48.3 | 1.29 | 0.04 | 1.70 | 89.5 | 1.27 | 0.00 | 1.22 |
| 132.6 | 1.61 | 0.36 | 1.22 | 129.2 | 1.68 | 0.42 | 1.13 | 57.2 | 1.30 | 0.04 | 1.78 | 105.0 | 1.28 | 0.01 | 1.32 |
| 165.9 | 1.70 | 0.45 | 1.03 | 181.1 | 1.81 | 0.55 | 1.11 | 80.3 | 1.31 | 0.05 | 2.01 | 106.6 | 1.23 | 0.04 | 1.51 |
| 176.4 | 1.79 | 0.54 | 0.91 | 200.4 | 1.85 | 0.59 | 1.06 | 85.2 | 1.39 | 0.13 | 2.32 | 115.7 | 1.27 | 0.00 | 1.29 |
| 178.3 | 1.70 | 0.45 | 1.22 | 220.9 | 1.83 | 0.57 | 0.98 | 89.3 | 1.49 | 0.24 | 2.72 | 122.7 | 1.29 | 0.02 | 1.66 |
| 228.2 | 1.81 | 0.56 | 1.12 | 312.2 | 1.92 | 0.66 | 1.12 | 99.5 | 1.74 | 0.50 | 2.56 | 127.8 | 1.26 | 0.01 | 1.40 |
| 244.5 | 1.81 | 0.56 | 1.04 | | | | | 112.8 | 1.43 | 0.19 | 2.49 | 187.6 | 1.31 | 0.04 | 1.76 |
| 318.4 | 1.92 | 0.67 | 0.93 | | | | | 133.3 | 1.34 | 0.90 | 2.07 | | | | |
| 429.8 | 2.03 | 0.78 | 1.10 | | | | | 144.2 | 1.87 | 0.62 | 1.01 | | | | |
| | | | | | | | | 221.7 | 1.75 | 0.50 | 1.75 | | | | |
| | | | | | | | | 241.0 | 1.83 | 0.58 | 1.23 | | | | |

[a]Q, mmol OTC $kg^{-1}$ clay; $d_{001}$, nm; $\Delta d = d_{001}$(at Q > 0) − $d_{001}$ (at Q = 0); fwhm (full fixed-width at half-maximum intensity), $2\theta°$.

field.[34] Previous validation studies have shown that the COMPASS force field can provide for adequate simulations of a model MONT,[35] metal cation hydration,[36,37] and various organic molecules,[17,36−38] including hydrated OTC,[17] by providing bond lengths and bond angles in agreement with structural data of TET molecules.[39] Following the general procedure delineated by Aristilde et al.,[17] an annealing Monte Carlo approach with geometry optimization as implemented in the Adsorption Locator module of Materials Studio[40] was used first to obtain geometry-optimized conformations of the adsorptive molecules in the Na interlayer and in the OTC interlayer. A molecular dynamics relaxation step (up to 50 ps) at 298 K using the Forcite module in Materials Studio with the COMPASS force field was conducted next in order to obtain the final optimized structures of the adsorptive molecules (Figure 2); this simulation time was sufficient to optimize both the geometry and energy of the system as evidenced by equilibration in both the displacement and total energy profiles (data not shown). The $Z$ coordinates of the optimized structures of the adsorptive molecules were used subsequently for computing XRD profiles.

**Simulation of XRD Profiles.** The XRD profiles were simulated for a two-component system and different proportions of the Na and OTC interlayers. For the purpose of the XRD examination, the OTC interlayer was assumed to incorporate a constant and maximum amount of two OTC molecules per unit cell. It was not possible to use the XRD data to perform adequate constraints of the actual number of OTC molecules in the OTC interlayer due to the lack of well-defined peaks and a reduced number of observable reflections at high-angle regions. Moreover, interlayer Na cations and water molecules cannot be distinguished in XRD due to their similar scattering power; 42 and 58 interlayer $Na/H_2O$ species were introduced in Na and OTC interlayers, respectively, consistent with the aforementioned Monte Carlo simulations. Due to the limitations in obtaining structural information from the XRD data, no structural refinement and no data fitting were performed. Simulations were thus meant to explore the signature of the XRD profiles under different patterns of interstratification and to obtain qualitative similarity between calculated and experimental profiles. The effect of an imperfect interlayer electron density distribution is expected to be minor compared to the relative proportion of the different layer types and their stacking sequences.

The theoretical basis for the calculations of the simulated XRD profiles is detailed elsewhere;[41] general guidelines are given here. These calculations require the determination of the fractions of total interlayers consisting of either the Na interlayer or the OTC interlayer ($W_{Na}$ and $W_{OTC}$, respectively) and of the junction probabilities $P_{NaNa}$, $P_{NaOTC}$, $P_{OTCOTC}$, and $P_{OTCNa}$, wherein $P_{ij}$ is the junction probability of layer type $j$ to follow layer type $i$. The six parameters are related by the following four equations:

$$W_{Na} + W_{OTC} = 1 \quad (1)$$

$$P_{NaNa} + P_{NaOTC} = 1 \quad (2)$$

$$P_{OTCOTC} + P_{OTCNa} = 1 \quad (3)$$

$$W_{Na}P_{NaOTC} = W_{OTC}P_{OTCNa} \quad (4)$$

which then yield two independent variables. Therefore, two variables, typically a compositional parameter ($W_{NA}$ or $W_{OTC}$) and one junction probability (e.g., $P_{NaNa}$), are sufficient to describe the system. With dependence on the respective values of these two probability parameters, three mains patterns of interstratification can be defined: random, segregated, and ordered. When $P_{NaNa} = W_{Na}$, the occurrence of Na layers depends only on their relative proportion and not on the nature of the previous layer: the interstratification is characterized as random (or $R_0$). When $P_{NaNa} > W_{Na}$, the occurrence of a Na layer is favored if the previous layer is also a Na layer, thus promoting clustering of the two layer types, in which case the interstratification is said to be segregated; the tendency to segregation is estimated by the Sg parameter [$Sg = 1 - (1 - P_{NaNa})/(1 - W_{Na})$].[41] And, interstratification is ordered when $P_{NaNa} < W_{Na}$, thus indicating a dispersion of the minor layer type. Here, diffraction profiles corresponding to 100% Na interlayers and 100% OTC interlayers were calculated first


dx.doi.org/10.1021/la400598x | Langmuir 2013, 29, 4492−4501

followed by a series of calculations for the following: random interstratification and a partial segregation with Sg of 0.25. The following relationships were thus used to calculate XRD profiles for the two series of XRD patterns: $P_{NaNa} = W_{Na}$ for $R_0$; and $P_{NaNa} = (1 - Sg)W_{Na} + Sg$ with Sg = 0.25 (Supporting Information); XRD patterns were calculated for the entire compositional range ($W_{Na}$ = 0 to 1).

## RESULTS AND DISCUSSION

**Experimental Validation of Model Interlayer Environment.** It was previously suggested[42] that specific adsorptive conformation may be important to favor interaction of OTC species with clay mineral surface. Our previous exploratory computational investigation of the OTC adsorption in the model MONT interlayer at a spacing of 1.25, 1.40, 1.5, 1.6, 1.8, and 1.9 nm[17] revealed that at least a $d_{001}$ of 1.6 nm was required to allow intercalation of the OTC molecule within the model MONT interlayer. The most thermodynamically favorable adsorbate structures were obtained within a $d_{001}$ of 1.8 nm, which facilitates electrostatic interactions and both indirect (i.e., water-bridging) and direct H-bonding interactions of the intercalated OTC with the MONT tetrahedral sheets. These interactions were confirmed by NMR and IR spectroscopic measurements, and XRD analysis reveals an apparent $d_{001}$ of 1.83 nm at about 254 $\mu$mole OTC/g clay at pH 4, consistent with the proposed optimal layer spacing.[17]

In order to provide further experimental confirmation of the optimal layer spacing and probe the influence of pH, we examined the fwhm profile as a function of $d_{001}$ and amount of adsorbed OTC at pHs 4, 5, 6, and 8 (Table 1). Changes in fwhm have been attributed previously to the evolution of the different configurations of the intercalated molecules,[17,18] whereby, in a profile of fwhm values as a function of $d_{001}$, an increase in fwhm typically indicates interstratification of different layer types. Similar to the hypothesis put forth in the case of the adsorption of lysine on MONT,[18] a new minimum in fwhm would be reached when the clay interlayers are saturated with (or mostly contain) adsorbed OTC, and the corresponding layer spacing would be considered optimal for the binding of OTC in the interlayer. Under all our experimental conditions, there was an initial increase in fwhm as a function of $d_{001}$ (Table 1, Figure 3), a characteristic feature of mixed layers[43] where Na and OTC interlayers coexist. In lieu of random demixing, it was proposed previously[18] that changes in the position of the 001 peak may be due instead to a gradual change in the interlayer configuration occurring homogeneously within all layers, wherein the molecules would change position, for instance, from being parallel to the clay sheet to being perpendicular. However, the aforementioned requirement of a $d_{001}$ of 1.6 nm or greater in order to accommodate the intercalated OTC is not in agreement with this proposal. Also consistent with the coexistence of the two interlayer types, we previously observed, using $^{23}$Na NMR at pH 4,[17] undisturbed environments of interlayer Na cations at an amount of adsorbed OTC lower than the permanent structural charge of the clay. Here as the ratio of Na to OTC interlayer decreases, as characterized by a significant increase in $d_{001}$ as a function of adsorbed OTC at pHs 4, 5, and 6, the fwhm profiles given as a function of $d_{001}$ reaches a maximum followed by a steady decrease (Table 1, Figure 3). A minimum in fwhm was observed at an apparent $d_{001}$ of 1.79, 1.83, and 1.87 at pHs 4, 5, and 6, respectively (Table 1, Figure 3). After the minimum value of fwhm is reached at both pH 4 and pH 5, we note a slight increase in fwhm at higher $d_{001}$ values (Table 1, Figure 3), which we attributed to the loss of scattering coherence; the peak position may be shifted toward a low angle when the size of coherent scattering domains is reduced, due to decreasing structure factor in the low-angle regions.[41]

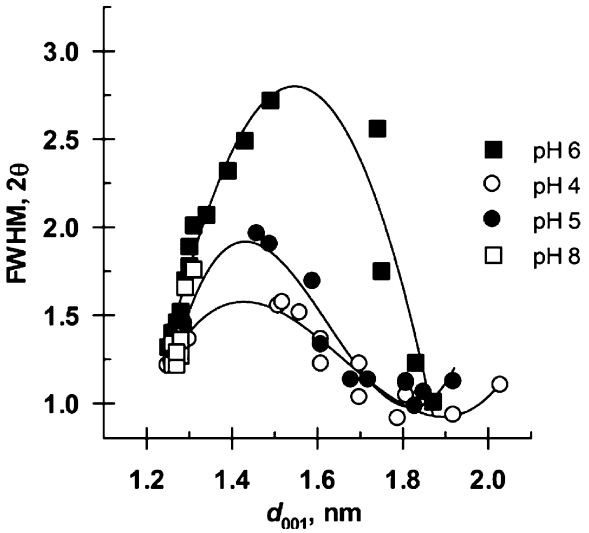


**Figure 3.** Changes in full-fixed width at half-maximum intensity (fwhm) as a function of apparent $d_{001}$ for OTC-clay samples at pH 4 (○), pH 5 (●), pH 6 (■), and pH 8 (□). The lines are intended as eye guides. The data from the X-ray diffractograms are shown in Table 1.

While OTC is increasingly anionic as pH increases (Figure 1), the high p$K_a$ (9.9) of the protonated dimethylamino group means that this moiety can still be involved in cation-exchange reactions to facilitate electrostatic interactions between OTC and the negatively charged clay surface, as corroborated by a reported change in the IR vibration bands of the dimethylamino group, upon interaction of OTC with MONT at both pH 4 and pH 8.[17] The same study[17] also reports that the $^1$H−$^{13}$C NMR signatures of the OTC adsorbed on MONT at both pH 4 and pH 8 imply a similar OTC binding configuration of OTC on the basal surface both within the interlayers and on external sites. These findings led us to hypothesize that, despite the different speciation of OTC, the presence of the positive charge from the protonated amino group may be dictating the OTC orientation on the clay surface, resulting in a similar interlayer binding environment for the OTC interlayers. In agreement with this hypothesis, the fwhm profiles at pHs 4, 5, and 6 exhibited a minimum at about the same $d_{001}$, thus implying a similar optimal environment for the OTC interlayers. These results led us to affirm that the $d_{001}$ of 1.8 nm is appropriate to construct the model adsorbate structures of the OTC interlayers; the layer spacing for the molecular modeling of the Na interlayers was chosen to be 1.2575 nm, the average apparent $d_{001}$ in the absence of OTC under our four experimental pH conditions (Table 1).

It is a common, though erroneous, assumption to deduce the optimal interlayer environment for intercalated TET and other molecules,[12,23,44] from any measured $d_{001}$. First, the interlayer environment is influenced by the RH conditions, which affect the hydration states of the smectite interlayers,[30] the interactions of the intercalated TET molecules with the clay surface,[17] and thus the apparent $d_{001}$.[12] For instance, a previous study[12] reported a different $d_{001}$ at two different RHs for the


dx.doi.org/10.1021/la400598x | Langmuir 2013, 29, 4492−4501

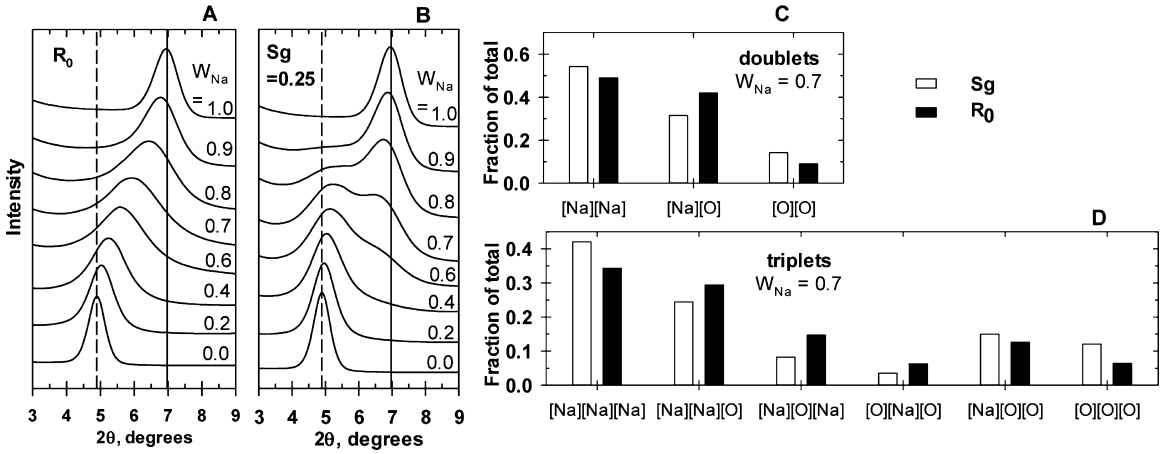


**Figure 4.** Simulated XRD profiles as a function of the fraction of Na interlayers ($W_{Na}$) for (A) random interstratification ($R_0$) and (B) partial segregation (Sg = 0.25) and the fraction of (C) layer pairs and (D) triplets, each of the total theoretical layer stacking composition at $W_{Na}$ = 0.7. In A and B, the solid vertical line indicates $d_{001}$ of 1.26 nm for Na interlayers and the dashed vertical line indicates $d_{001}$ of 1.8 nm for OTC interlayers. In C and D, the layer stackings for $R_0$ and Sg = 0.25 are shown as black and white bars, respectively; [Na] represents a Na interlayer and [O] represents an OTC interlayer. See the Supporting Information for the fraction of layer pairs and triplets at $W_{Na}$ = 0.8 and $W_{Na}$ = 0.6.

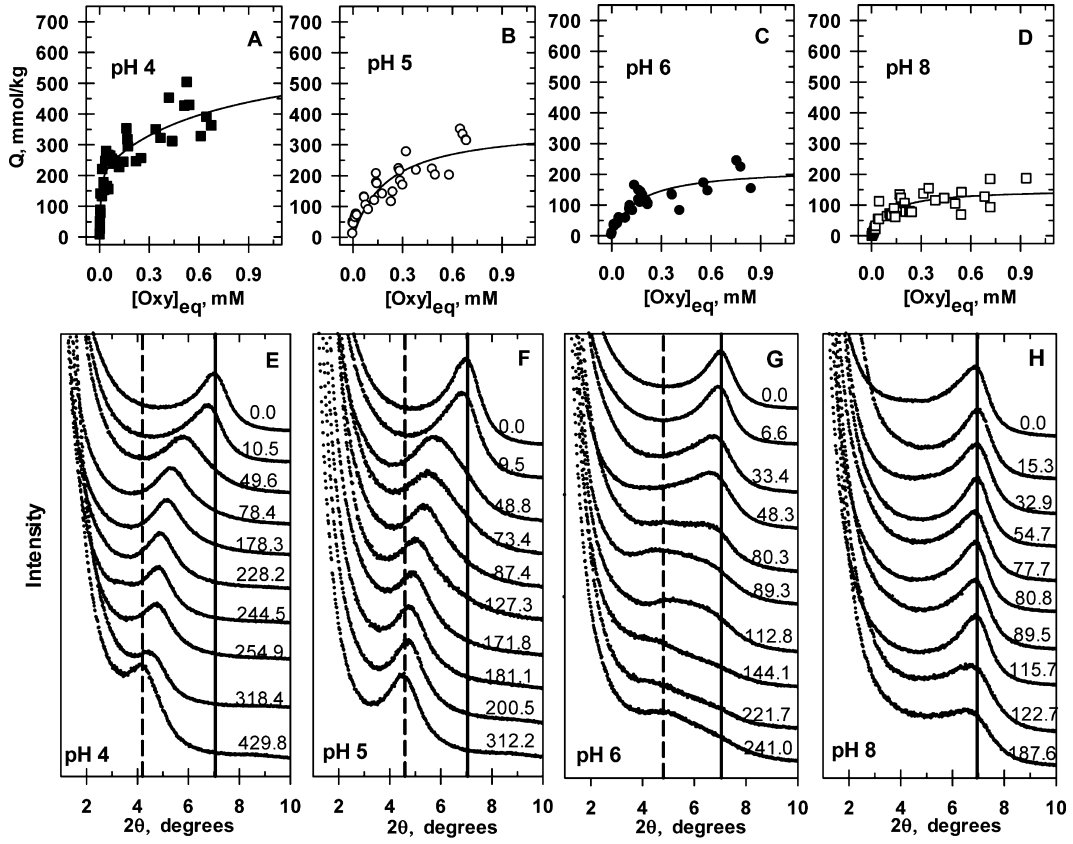


**Figure 5.** Amount of adsorbed OTC (Q, mmol OTC $kg^{-1}$) vs equilibrium OTC concentration in solution ($[OTC]_{eq}$, mmol OTC $L^{-1}$) at (A) pH 4, (B) pH 5, (C) pH 6, and (D) pH 8 and selected X-ray diffraction patterns of OTC–MONT at (E) pH 4, (F) pH 5, (G) pH 6, and (H) pH 8. In A–D, the lines are meant as eye guides. In E–H, the numbers indicate the Q values measured for the OTC–clay suspensions in mmol OTC $kg^{-1}$ clay; the solid vertical lines indicate apparent $d_{001}$ of 1.25, 1.26, 1.25, and 1.27 nm at (E) pH 4, (F) pH 5, (G) pH 6, and (H) pH 8, respectively, and the dashed vertical lines indicate apparent $d_{001}$ of 2.03, 1.92, and 1.83 nm at (E) pH 4, (F) pH 5, and (G) pH 6, respectively. At low 2$\theta$, the actual $d_{001}$ values may be significantly lower than apparent ones, because of small sizes of the coherent scattering domains. The data from all the measured X-ray diffractograms are shown in Table 1.

same amount of adsorbed TET antibiotics. Therefore, XRD data should be obtained under a specific RH condition, and conclusions made about the interlayer spacing only apply to that specific condition. Second, as demonstrated and discussed above, both the $d_{001}$ and fwhm values should be taken into consideration in order to make any assertion on the interlayer binding environment of the intercalated molecule. It is necessary to have the interlayers saturated (or mostly


dx.doi.org/10.1021/la400598x | Langmuir 2013, 29, 4492–4501

populated) with the intercalated organic molecule in order to attribute the measured apparent $d_{001}$ to the optimal spacing requirement for the interlayer adsorption of the molecule. Whereas an increase in $d_{001}$ indicates the presence of the guest molecule in the interlayer, the profile of fwhm as a function of $d_{001}$ allows, in the present case, for monitoring the evolution of the interlayers' population from only Na, both Na and OTC, to only (or mostly) OTC (Figure 3).

**Simulation of XRD Profiles.** The coordinates of the optimized interlayer adsorptive structures (Figure 2) were employed to simulate XRD patterns (Figure 4), by assuming either random or segregated interstratification of the Na- and OTC interlayers. In the case of random interstratification, the simulated profiles illustrate a low-angle asymmetry of the ∼1.26 nm peak ($2\theta$ = 7°), at first upon decreasing the relative proportion of Na interlayers to $W_{Na}$ = 0.9. Further decrease in the relative proportion of Na interlayers (i.e., decreasing $W_{Na}$) induces a steady shift of the peak toward lower angles, accompanied by a significant broadening. The latter is reduced as the peak migrates to the peak position ($2\theta \approx 5°$), corresponding to the $d_{001}$ of the OTC interlayers (Figure 4A). In the case of segregated interstratification, there was a different evolution of the simulated peak profile as a function of decreasing $W_{Na}$, whereby at $W_{Na} < 0.9$, two maxima coexist: one at 5° $2\theta$ and another at 7° $2\theta$. Both peaks are asymmetrical and slightly shifted compared to their ideal positions (Figure 4B). These two maxima persist as long as Na interlayers prevail in the structure at $W_{Na} \geq 0.6$, whereas, at lower $W_{Na}$, increasing the OTC interlayers result in a single peak positioned at 5° $2\theta$ with a strong high-angle asymmetry, which decreases with an increasing proportion of the OTC interlayers (Figure 4B).

The theoretical compositional signature of the simulated XRD profiles provides insight into the different layer stacking arrangements between random and segregated interstratification of the interlayers (Figure 4, panels C and D, and the Supporting Information). Consistently, we note that the randomly interstratified mixed layers have higher proportion of layer pairs and triplets with diverse composition, characterized by [Na][O], [Na][Na][O], and [O][Na][O] than the segregated mixed layers, whereas segregated interstratification leads to higher proportion of layer pairs and triplets with similar composition, characterized by [Na][Na], [O][O], [Na][Na][Na], [Na][O][O], and [O][O][O], than the randomly interstratified mixed layers, where [Na] is a Na-interlayer and [O] is an OTC-interlayer (Figure 4C and 4D and the Supporting Information). The occurrence of pairs and triplets of identical layers, which is favored in the case of segregated interstratification, is thus responsible for the aforementioned coexistence of two maxima, corresponding to the two periodic end-members (Figure 4B).

**Adsorption and Interstratification as a Function of pH.** As previously reported,[17] the amount of OTC adsorbed decreases with increasing pH. Here, the plots of adsorbed OTC (Q) as a function of equilibrium OTC concentration ([$OTC_{eq}$]) indicate that the decrease in the adsorption capacity of MONT for OTC with increasing pH correlates positively with the ability of OTC to intercalate within the MONT layers as revealed by XRD (Figure 5). We systematically monitor the XRD patterns as a function of both Q and pH. At all the experimental pH, an increase in Q eventually results in a positional shift of the basal reflections as indicated by an increase in $d_{001}$, but the XRD profiles differ as a function of pH (Table 1, Figure 5, panels E–H). By contrast to the clear evidence of intercalation obtained at pHs 4, 5, and 6, there is no peak shift at pH 8, indicative of no intercalation of OTC, except at a high loading at Q ≥ 122.7 mmol OTC $kg^{-1}$ clay, whereby there is an increase in fwhm accompanied by an appreciable asymmetry of the low-angle side of the 1.27 nm peak peak (∼$2\theta$ = 7°) (Table 1and Figure 5, panels E–H). However, despite the minimal amount of OTC present in the MONT interlayers at pH 8, there is still significant OTC adsorption (Figure 5D), which must essentially occur on external basal sites and edge sites deprotonated at circumneutral and higher pH values,[45−48] as we noted previously, while the overall OTC molecule is anionic at pH 8, the cationic moiety is still present to be involved in electrostatic interactions with negatively charged sites.

On the basis of the similarity with the simulated profiles depicted in Figure 4 (panels A and B), the XRD patterns measured at pHs 4 and 5 (Figure 5, panels E and F) reflect random interstratification of Na and OTC interlayers, whereas the XRD pattern at pH 6 is indicative of partially segregated interstratification of these interlayers (Figure 5G). Accordingly, at both pH 4 and 5, a unique 001 peak shifts steadily from ∼7° to 4−4.5° $2\theta$. This peak exhibits first a low-angle asymmetry, and then a significant broadening, followed by a decreasing high-angle asymmetry as the peak sharpens again (Figures 3 and 5, panels E and F). At pH 6, as was observed at pHs 4 and 5, there was initially one 001 peak with a low-angle asymmetry (Figure 5G) for the lower values of Q (up to 48.3 mmol OTC $kg^{-1}$ clay), but a subsequent increase of Q resulted in different XRD profiles. At higher Q values, there is a doublet at ∼1.25 and ∼1.83 nm, which is characteristic of crystals or domains containing essentially either Na interlayers or OTC interlayers, respectively, both types of interlayers being mutually exclusive (Figure 5G). An increase in the amount of adsorbed OTC results in a modification of the relative intensities of the two peaks, as indicated by a steady increase of the 1.83 nm peak at the expense of that at 1.26 nm. This change in the two peaks was also illustrated as a function of decreasing $W_{Na}$ (i.e., decreasing the fraction of Na interlayers) in the simulated XRD profiles with the segregated interstratification pattern (Figure 4).

While the aqueous speciation of OTC does not differ much from pH 5 to pH 6, as more than 96% of the OTC species are zwitterionic (Figure 1B), there was consistently more intercalated OTC in the MONT layers at pH 5 than at pH 6 for similar Q values (Figures 4F and 5G). From the simulated profile (Figure 4, panels A and B), we estimated the fraction of the total interlayers with intercalated OTC at about the same Q values: at pH 5, there were about 35% and 50% OTC interlayers at 48.8 and 87.4 mmol OTC $kg^{-1}$ clay, respectively, whereas at pH 6, there were about 15% and 30% OTC interlayers at 48.3 and 89.3 mmol OTC $kg^{-1}$ clay, respectively (Figure 5, panels F and G). Our findings at pH 6 thus indicate that, compared to pH 5, not only sorption on external sites is favored over intercalation in the smectite interlayers but also the intercalated OTC molecules are segregated in specific domains of the clay crystals (Table 1and Figure 5, panels F and G). These results further imply that, in addition to favorable speciation of the antibiotic species, the pH-dependent intercalation of TET and related antibiotics may be influenced by the changes in the access of OTC to the clay interlayers as a function of pH. As pointed out in the Introduction, a previous study of OTC adsorption on a MONT clay[15] showed XRD patterns where there was one single 001 peak for interlayer


dx.doi.org/10.1021/la400598x | Langmuir 2013, 29, 4492−4501

adsorption under acidic pH conditions but two peaks were observed at higher pH values, further pointing out that the segregation of the interstratified interlayers is promoted as pH increases.

We acknowledge that the measured XRD patterns reflect the structures of the MONT layers in oriented films under low hydration (RH = 20%) and may not be characteristic of these layers in suspension.[49,50] Here, the theoretical layer stacking sequences deduced from simulated XRD implicitly inform on the accessibility of OTC to the MONT interlayers, as reflected in their oriented arrangements depicted by the measured XRD patterns (Figure 4 and Figure 5). There are two ways to envisage the sorption process responsible for the pH-dependent OTC intercalation within the MONT layers, either the OTC binding on external sites under circumneutral and higher pH conditions prevents exfoliation of the MONT layers or the exfoliation of the MONT layers solely is pH-dependent such that exfoliation is significantly high or complete at acidic pH but minimal at basic pH. We exclude the first scenario because it does not explain how, by preventing binding to vicinal interlayers, OTC binding to external sites could promote the clustering of Na or OTC interlayers, in order to generate the observed segregated pattern of interstratification. We thus hypothesize that the second scenario is the likely sorption process, whereby exfoliation of the MONT layers is incomplete at circumneutral and higher pH values, in which case OTC minimal intercalation is due to decreased OTC access to exfoliated layers such that OTC binding is thus limited to the external sites of these smectite crystallites or unexfoliated platelets. This scenario also implies preferential binding of OTC to exfoliated layers over Na, which is likely due to the ability of OTC to be engaged, in addition to electrostatic interactions, in multiple H-bonding interactions with the clay surface.[17]

## CONCLUSION

Observed changes in XRD patterns have implied pH-dependent intercalation of antibiotics within smectites, but characterization of the resulting interstratified structures is largely lacking. In the present study, we employed both simulated and experimental XRD in an effort to characterize these structures, following the interlayer adsorption of OTC within a Na-montmorillonite as a function of pH. Our results demonstrate that the intercalation of the antibiotic species within the smectite layers at low acidic pH is random, but as pH increases, intercalation is both decreased and segregated. The formation of smectite quasi-crystals (or incomplete exfoliation of smectite layers), characterized by the formation of aggregated smectite interlayers, was proposed previously.[49−51] The clustering of Na-smectite layers with reduced access of OTC to the unexfoliated smectite layers are consistent with this phenomenon predominating at circumneutral and basic pH values. The scope of our data precludes the determination of the specific mechanisms underlying this pH-dependent promotion in particle aggregation. However, our XRD data show that the pH-dependent change in the access of OTC to the clay interlayers is not positively correlated to OTC speciation, thus corroborating a possible correlation to changes in the clay surface chemistry as pH increases. In terms of environmental relevance, we acknowledge that the adsorbed concentrations used in our study exceed what are found for TETs in natural soils,[52] but the low pH and high antibiotic concentration required for interlayer adsorption both suggest that the intercalation of these antibiotics and other low-level related contaminants within minerals in the soil environment is likely limited due to unfavorable aqueous conditions and competition from the abundant presence of natural organic matter molecules in soils. In terms of implications for engineered systems using smectite-type minerals to capture polar or ionizable organic molecules, our findings suggest that, under circumneutral and basic pH conditions, the physical exclusion of these molecules may be minimal, and that the adsorbed molecules may instead primarily populate the external sites of the minerals. In sum, depending on the aqueous conditions and the type of organic adsorptive and clay minerals, the phenomenon presented here may have important implications for the sequestration of soil organic matter, the environmental fate and bioavailability of organic contaminants, and the dynamics of engineered organo-clay composites.

## ASSOCIATED CONTENT

### Supporting Information

Junction probability of a Na interlayer to follow another Na interlayer ($P_{NaNa}$) as a function of fraction Na interlayers ($W_{Na}$). Fraction of layer pairs and triplets each of the total theoretical layer stacking composition at $W_{Na}$ = 0.8 and $W_{Na}$ = 0.6. This material is available free of charge via the Internet at http://pubs.acs.org.

## AUTHOR INFORMATION

### Corresponding Author

*E-mail: la31@cornell.edu.

### Author Contributions

L.A., B.L., and L.C. designed the research. L.A. performed the molecular modeling simulations, the adsorption experiments, and the XRD measurements. B.L. performed the simulated XRD profiles. L.A. and B.L. analyzed the data. L.A., B.L., and L.C. wrote the manuscript. All authors have given approval for the final version of the manuscript.

### Notes

The authors declare no competing financial interest.

## ACKNOWLEDGMENTS

We are grateful to Audrey Perrier and Florian Molton of the University of Grenoble for technical assistance and to Ian C. Bourg for helpful comments during the preparation of this manuscript. L.A. and L.C. acknowledge a Fulbright Scholarship and a CNRS Scholarship, respectively. We thank three anonymous reviewers for their insightful comments.

## REFERENCES

(1) Glaeser, R.; Méring, J. Isothermes d'hydration des montmorillonites bi-ioniques (Na, Ca). *Clay Miner. Bull.* **1954**, *2*, 188−193.

(2) McAtee, J. L. Heterogeneity of montmorillonite. *Clays Clay Miner.* **1956**, *5*, 279−288.

(3) Fink, D. H.; Nakayama, F. S.; McNeal, B. L. Demixing of exchangeable cations in free-swelling bentonite clay. *Soil Sci. Soc. Am. Proc.* **1971**, *35*, 552−555.

(4) Shainberg, I.; Alperovitch, N. I.; Keren, R. Charge density and Na-K-Ca exchange on smectites. *Clays Clay Miner.* **1987**, *35*, 68−73.

(5) Iwasaki, T.; Watanabe, T. Distribution of Ca and Na ions in dioctahedral smectites and interstratified dioctahedral mica/smectites. *Clays Clay Miner.* **1988**, *36*, 73−82.

(6) Ferrage, E.; Tournassat, C.; Rinnert, E.; Lanson, B. Influence of pH on the interlayer cationic composition and hydration state of Ca-montmorillonite: Analytical chemistry, chemical modelling and XRD

profile modelling study. *Geochim. Cosmochim. Acta* **2005**, *69*, 2797−2812.
(7) Möller, M. W.; Hirsemann, D.; Haarmann, F.; Senker, J.; Breu, J. Facile scalable synthesis of rectorites. *Chem. Mater.* **2010**, *22*, 186−196.
(8) Lanson, B. Modelling of X-ray diffraction profiles: Investigation of defective lamellar structures crystal chemistry. In *European Mineralogical Union Notes in Mineralogy, Layered mineral structures and their applications in advanced technologies*; Brigatti, M. F. and Mottana, A. Eds., European Mineralogical Union & Mineralogical Society UK & Ireland: London, 2011; Vol. *11*, Chapter 4.
(9) McBride, M. B; Mortland, M. M. Segregation and exchange properties of alkylammonium ions in a smectite and vermiculite. *Clays Clay Miner.* **1973**, *21*, 323−329.
(10) Maes, A.; Cremers, A. Mixing-demixing behavior of calcium-ethylammonium mixtures in Otay montmorillonite. *Clays Clay Miner.* **1983**, *31*, 71−73.
(11) McBride, M. B; Mortland, M. M. Surface properties of mixed Cu(II)-tetraalkylammonium montmorillonites. *Clay Miner.* **1975**, *10*, 357−368.
(12) Pils, J.; Laird, D. A. Sorption of tetracycline and chlortetracycline on K- and Ca-saturated soil clays, humic substances and clay-humic complexes. *Environ. Sci. Technol.* **2007**, *41*, 1928−1933.
(13) Chang, P.-H.; Jean, J.-S.; Jiang, W.-T.; Li, Z. Mechanisms of tetracycline on rectorite. *Colloid Surf., A* **2009**, *339*, 94−99.
(14) Li, Z.; Kolb, V. M.; Jiang, W.-T.; Hong, H. FTIR and XRD investigations of tetracycline intercalation in smectites. *Clays Clay Miner.* **2010**, *4*, 462−474.
(15) Kulshrestha, P.; Giese, R. F., Jr.; Aga, D. S. Investigating the molecular interactions of oxyteracycline in clay and organic matter: Insights on factors affecting its mobility in soil. *Environ. Sci. Technol.* **2004**, *38*, 4097−4105.
(16) Aristilde, L.; Marichal, C.; Miéhé-Brendlé, J.; Lanson, B.; Charlet, L. Interactions of oxytetracycline with a smectite clay: A spectroscopic study with molecular simulations. *Environ. Sci. Technol.* **2010**, *44*, 7839−7845.
(17) Wang, C.; Ding, T.; Teppen, B. J.; Boyd, S. A.; Song, C.; Li, H. Role of interlayer hydration in lincomycin sorption by smectite clays. *Environ. Sci. Technol.* **2009**, *43*, 6171−6176.
(18) Parbhakar, A.; Cuadros, J.; Sephton, M. A.; Dubbin, W.; Coles, B. J.; Weiss, D. Adsorption of L-lysine on montmorillonite. *Colloids Surf., A* **2007**, *307*, 142−149.
(19) Chander, Y.; Kumar, K.; Goyal, S. M.; Gupta, S. C. Antibacterial activity of soil-bound antibiotics. *J. Environ. Qual.* **2005**, *34*, 1952−1957.
(20) Pinck, L. A.; Soulides, D. A.; Allison, F. E. Antibiotics in soils: II. Extent and mechanism of release. *Soil Sci.* **1961**, *91*, 94−99.
(21) Sithole, B. B.; Guy, R. D. Models for tetracycline in aquatic environments. *Water, Air, Soil Pollut.* **1987**, *32*, 315−321.
(22) Parolo, M. E.; Savini, M. C.; Vallés, J. M.; Baschini, M. T.; Avena, M. J. Tetracycline adsorption on montmorillonite: pH and ionic strength effects. *Appl. Clay Sci.* **2008**, *40*, 179−186.
(23) Figueroa, R. A.; Leonard, A.; Mackay, A. A. Modeling tetracycline antibiotic sorption to clays. *Environ. Sci. Technol.* **2004**, *38*, 476−48.
(24) Wang, Y. J.; Jia, D.-A.; Sun, R.-J.; Zhu, H.-W.; Zhou, D.-M. Adsorption and cosorption of tetracycline and copper(II) on montmorillonite as affected by solution pH. *Environ. Sci. Technol.* **2008**, *42*, 3254−3259.
(25) Porubcan, L. S.; Serna, C. J.; White, J. L.; Hern, S. L. Mechanism of adsorption of clindamycin and tetracycline by montmorillonite. *J. Pharm. Sci.* **1978**, *67*, 1081−1087.
(26) Wang, C.-J.; Li, Z.; Jiang, W.-T.; Jean, J.-S.; Liu, C.-C. Cation exchange interaction between antibiotic ciprofloxacin and montmorillonite. *J. Hazard. Mater.* **2010**, *183*, 309−314.
(27) Bourg, I. C.; Sposito, G. Ion exchange phenomena. In *Handbook of Soil Science, Properties and Processes*, 2nd ed.; Huang, P. M., Li, Y., Summer, M. E., Eds.; CRC Press: Boca Raton, 2011; Chapter 16.
(28) Reinholdt, M.; Miéhé-Brendlé, J.; Delmotte, L.; Le Dred, R.; Tuilier, M.-H. Synthesis and characterization of montmorillonite-type phyllosilicates in a fluoride medium. *Clay Miner.* **2005**, *40*, 177−190.
(29) Reinholdt, M.; Miéhé-Brendlé, J.; Delmotte, L.; Tuilier, M.-H.; Le Dred, R.; Cortès, R.; Flank, A.-M. Fluorine route synthesis of montmorillonite containing Mg or Zn and characterization by XRD, thermal analysis, MAS NMR, and EXAFS spectroscopy. *Eur. J. Inorg. Chem.* **2001**, *11*, 2831−2841.
(30) Ferrage, E.; Lanson, B.; Sakharov, B. A.; Drits, V. A. Investigation of smectite hydration properties by modeling experimental X-ray diffraction patterns: Part I. Montmorillonite hydration properties. *Am. Mineral.* **2005**, *90*, 1358−1374.
(31) Géhin, A.; Grenèche, J.-M.; Tournassat, C.; Brendlé, J.; Rancourt, D.; Charlet, L. Reversible surface-sorption-induced electron transfer oxidation of Fe(II) at reactive sites on a synthetic clay mineral. *Geochim. Cosmochim. Acta* **2007**, *71*, 863−876.
(32) Berendsen, H. J. C.; Grigera, J. R.; Straatsma, T. P. The missing term in effect pair potentials. *J. Phys. Chem.* **1987**, *91*, 6269−6271.
(33) Cygan, R. T.; Liang, J.-J.; Kalinichev, A. G. Molecular models of hydroxide, oxyhydroxide, and clay phases and the development of a general force field. *J. Phys. Chem. B* **2004**, *108*, 1255−1266.
(34) Sun, H. COMPASS: An ab initio force-field optimized for condensed phase applications-overview with details on alkane and benzene compounds. *J. Phys. Chem. B* **1998**, *102*, 7338−7364.
(35) Sutton, R.; Sposito, G. Molecular simulation of humic substance-Ca-montmorillonite complexes. *Geochim. Cosmochim. Acta* **2006**, *70*, 3566−3581.
(36) Sutton, R.; Sposito, G.; Diallo, M. S.; Schulten, H.-R. Molecular simulation of a model of dissolved organic matter. *Environ. Toxicol. Chem.* **2005**, *24*, 1902−1911.
(37) Aristilde, L.; Sposito, G. Molecular modeling of metal complexation by a fluoroquinolone antibiotic. *Environ. Toxicol. Chem.* **2008**, *27*, 2304−2310.
(38) Aristilde, L.; Sposito, G. Binding of ciprofloxacin by humic substances: A molecular dynamics study. *Environ. Toxicol. Chem.* **2010**, *29*, 90−98.
(39) Koziol, A. E.; Davis, J.; Palenik, R. C.; Palenik, G. J. Structural studies of two tetracyclines: 4-dedimethylaminotetracycline hydrate and 6-methylene-5-oxytetracycline hydrochloride. *J. Crystallogr. Spectrosc. Res.* **1992**, *22*, 493−501.
(40) *Materials Studio*, version 4.2; Accelrys Corporation: San Diego, CA, 2001.
(41) Drits, V. A.; Tchoubar, C. *X-ray Diffraction by Disordered Lamellar Structures: Theory and Applications to Microdivided Silicates and Carbons*; Springer-Verlag: Berlin, 1990; p 371.
(42) Carasquillo, A. J.; Bruland, G. L.; MacKay, A. A.; Vasudevan, D. Sorption of ciprofloxacin and oxytetracycline zwitterions to soils and soil minerals: Influence of compound structure. *Environ. Sci. Technol.* **2008**, *42*, 7634−7642.
(43) Méring, J. L'interférence des rayons-X dans les systèmes à stratification désordonnée. *Acta Crystallogr.* **1949**, *2*, 371−377.
(44) Pei, Z.; Shan, X.-Q.; Kong, J.; Wen, B.; Owens, G. Coadsorption of ciprofloxacin and Cu(II) on montmorillonite and kaolinitie as affected by solution pH. *Environ. Sci. Technol.* **2010**, *44*, 915−920.
(45) Bourg, I. C.; Sposito, G.; Bourg, A. C. M. Modeling the acid-base surface chemistry of montmorillonite. *J. Colloid Interface Sci.* **2007**, *312*, 297−310.
(46) Charlet, L.; Schindler, P. W.; Spadini, L.; Furrer, G.; Zysset, M. Cation adsorption on oxides and clays: The aluminum case. *Aquat. Sci.* **1993**, *55*, 291−303.
(47) Wanner, H.; Albinsson, Y.; Karnland, O.; Wieland, E.; Wersin, P.; Charlet, L. The acid base chemistry of montmorillonite. *Radiochimica* **1994**, *66/67*, 157−162.
(48) Tournassat, C.; Ferrage, E.; Poinsignon, C.; Charlet, L. The titration of clay minerals. Part II. Structural-based model and implications for clay reactivity. *J. Colloid Interface Sci.* **2004**, *273*, 234−246.
(49) Pereira, T. R.; Laird, D. A.; Thompson, M. L.; Johnston, C. T.; Teppen, B. J.; Li, H.; Boyd, S. A. Role of smectite quasicrystal

dynamics in adsorption of dinitrophenol. *Soil Sci. Soc. Am. J.* **2008**, *72*, 347−355.
(50) Hui, L.; Pereira, T. R.; Teppen, B. J.; Laird, D. A.; Johnston, C. T.; Li, H.; Boyd, S. Ionic strength-induced formation of smectite quasicrystals enhances nitroaromatic compound sorption. *Environ. Sci. Technol.* **2007**, *41*, 1251−1256.
(51) Sposito, G. *The Chemistry of Soils*; Oxford University Press: New York, 2008.
(52) Sarmah, A. K.; Meyer, M. T.; Boxall, A. B. A. A global perspective on the use, sales, exposure pathways, occurrence, fate, and effects of veterinary antibiotics (VAs) in the environment. *Chemosphere* **2006**, *65*, 725−759.